Available online at www.sciencedirect.com
ScienceDirect
Applied Catalysis B: Environmental 81 (2008) 258–266
APPLIED CATALYSIS B: ENVIRONMENTAL
www.elsevier.com/locate/apcatb

Structure and performance of a novel TiO_2-phosphonate composite photocatalyst

P. Raja [a], V. Nadtochenko [b], U. Klehm [c], J. Kiwi [a,*]

[a] *Department of Chemistry, Laboratory of Photonics and Interfaces, Institute of Chemical Sciences and Engineering, Swiss Federal Institute of Technology, Lausanne 1015, Switzerland*
[b] *Laboratory of Fast Kinetics, Russian Academy of Sciences, Chernogolovka, Moscow region 142432, Russia*
[c] *Aqura GmbH, AQ-EM, Rodenbacher Ch. 4, D-6347 Hanau, Germany*

Received 15 October 2007; received in revised form 13 December 2007; accepted 16 December 2007
Available online 28 December 2007

Abstract

An innovative SiO_2-PO_4^{3-}-TiO_2 photocatalyst is presented which is able to bond TiO_2 to Raschig rings (RR). Evidence for the formation on the catalyst surface of P═O stretching bands near 1200–1250 cm^{-1} is presented by FTIR spectroscopy. The TiO_2 Degussa P25 on the catalyst surface (RR) was further characterized by high-resolution transmission electron microscopy (HRTEM), and X-ray diffraction showing that the composite catalyst prepared at 500 °C does not alter the particle size or crystallographic composition of the TiO_2 Degussa P25 particles. The Ti- and P-distribution of the catalyst surface overlayers was obtained by Ar-sputtering eroding up to 100 topmost catalyst layers. By atomic force microscopy (AFM) the root mean square roughness (Rq) or rugosity of ~771 nm and an average height of the catalyst layer of 1.52 μm were found on the glass surface. The root mean square roughness Rq varies very little in value before and after the photocatalysis indicating that the sample porosity is conserved during 4-CP photodegradation. The disappearance kinetics of 4-chlorophenol (4-CP) on the SiO_2-PO_4^{3-}-TiO_2 composite occurred within 15 min and was faster than the 45 min needed with suspensions of TiO_2 Degussa P25 (1 g L^{-1}). The SiO_2-PO_4^{3-}-TiO_2 photocatalyst was able to degrade repetitively 4-CP solutions without loss of activity. The effect of the light intensity, oxidant concentration and 4-CP concentration on the photodegradation kinetics was investigated and is reported in this study.

Keywords: Photocatalysis; SiO_2-PO_4^{3-}-TiO_2 composite photocatalyst; IR; Electron microscopy (HRTEM); XPS; NMR; Atomic force microscopy (AFM); Elemental analysis (EA); 4-Chlorophenol (4-CP)

1. Introduction

The phosphonic acid is used as an interfacial agent between the glass and the semiconductor, and its application has grown considerably during the last decade [1–4]. When used to graft TiO_2 on glass surfaces, phosphonic acids exhibit several advantages like: (a) phosphonic acids have no optical absorbance in the range of the TiO_2 photo-activity, (b) they are chemically non-reactive (inert) and (c) they are non-toxic and thermally stable. In particular, the grafting of functionalized phosphonic acids has been useful in the area of catalysis [2] and biomaterials [3,4]. The phosphonates transform themselves into phosphates during the high temperature required to bind TiO_2 on the glass surface. This study will provide some insight by IR-spectroscopy and NMR of the functional groups involved in the TiO_2 bond through PO_4^{3-} catalyst bonding. The depth of the PO_4^{3-} and TiO_2 layers into the glass was investigated by XPS through surface erosion measurements. In this study, we also suggest a comprehensive physical picture for the positioning of the surface layer elements on the silica glass surface.

TiO_2 photocatalysis is a valid alternative to more conventional waste-water treatment technologies since light with $\lambda < 400$ nm generates a valence band-hole positive enough to produce highly oxidative radicals and a conduction band-electron negative enough to reduce O_2 [5,6]. We have worked for some years on the immobilization of TiO_2 on many supports like: polymer films [7], plastics and Raschig rings (RR) [8]. Supported photocatalysts eliminate the need for post-treatment removal needed when suspensions of TiO_2 are used to abate

* Corresponding author. Tel.: +41 21 693 36 21; fax: +41 21 693 41 11.
E-mail address: John.Kiwi@epfl.ch (J. Kiwi).

0926-3373/$ – see front matter © 2008 Elsevier B.V. All rights reserved.
doi:10.1016/j.apcatb.2007.12.015

pollutants in aqueous media [5,6]. Immobilized TiO_2 degrade pollutants with acceptable kinetics not leaching out of the support and conserving their long-term operational efficiency [9–11].

Chlorocarbons in aqueous solutions like 4-CP have been recognized as a threat to human health by the US EPA [12], and a comprehensive review by Esplugas and co-workers has appeared referencing the studies to abate this compound by TiO_2 photocatalysis [13]. Our laboratory has recently reported the degradation of chlorophenols with TiO_2 suspensions activated under mercury light irradiation [14,15]. The present study focuses on a composite photocatalyst (SiO_2-PO_4^{3-}-TiO_2) and to show its stability and efficiency during long-term operation. The addition of the oxidant (H_2O_2) was to increase the mineralization of 4-CP to CO_2, water and HCl.

This study has the objective of showing the performance of an innovative composite photocatalyst using phosponic acid to bond TiO_2 on glass surface (RR).

2. Experimental

2.1. Materials

The 4-chlorophenol (4-CP), acids, bases and H_2O_2 were Fluka p.a. and used as received. The TiO_2 Degussa P25 photocatalyst was a gift from Degussa AG Switzerland, 6340 Baar. The RRs used were 4 mm × 4 mm made out of soda lime glass (thickness 1 mm). The soda lime glass used was made up by: 70% SiO_2, 10%(Na_2O, CaO, MgO K_2O) and 5% (Fe_2O_3, Al_2O_3). The reagent 1-teradecyl-phosphonic acid $CH_3(CH_2)_{13}P(O)(OH)_2$, FW 278.37 was Alfa Aesar and used as received. Other phosphonic acids with hydrocarbon chains of different length were assayed as interfacial agents to charge negatively the RRs surface during the catalyst preparation but the phosphonic reagent selected provided the best performance during the degradation of 4-CP.

2.2. Catalysts preparation

The RRs were washed with detergent and etched with HF 5%, for 10 min at 50 °C. After rinsing with bi-distilled water, they were immersed in 1-tetradecyl-phosphonic acid dissolved in methanol (50 g L^{-1}) for 2 h, then drained and dried overnight at room temperature. The rings were then dipped in a well-dispersed TiO_2 Degussa P25 suspension (5 g L^{-1}) and dried at 110 °C for 1 h. The pH of the TiO_2 suspension was ~4.2. At this pH, the surface of TiO_2 is positively charged since the isoelectric point of TiO_2 Degussa P25 is 7.0 [5,6]. This allows the electrostatic binding of the TiO_2 with the negative phosphonic-coated surface of the Raschig glass rings. The coating with TiO_2 was repeated a second time to cover regions that were not covered during the first dip coating. Then the rings were heated at 100 °C in air and subsequently for different time periods at 500 °C to diffuse the TiO_2 into the silica glass. Finally, the loaded glass rings were washed to eliminate the loosely bound TiO_2 particles from the SiO_2-PO_4^{3-}-TiO_2 composite surface.

2.3. Irradiation procedures

The photodegradation of 4-CP was carried out in small batch cylindrical photochemical reactors made from Pyrex glass (cut-off λ = 290 nm) of 70 mL capacity containing 50 mL aqueous solution. A grid was positioned close to the bottom of the photochemical reactor. The RRs were put above this grid and the stirrer below. An amount of 30 g TiO_2-coated RRs was introduced in the reactor. The vessels were irradiated with a medium pressure mercury lamp (400 W) from Photochemical Reactor Ltd. (Blounts Farm, Reading, Berkshire, UK) provided with a water-cooling jacket. The lamp had a bandwidth from 260 to 435 nm. The main emission wavelength was at 366 nm. The lamp was immersed in quartz well. The radiation field was 360° with 2.5×10^{19} photons s^{-1}. The integral radiant flux of the medium pressure mercury lamp reaching the reactor vessel wall was measured with a power-meter (YSI Corp. Colorado, USA). The incident light flux reaching the reactor wall emitted by the mercury lamp (400 W) was varied by using iron-grid filters with mesh size diameters of 0.15 and 0.6 mm. The 4-CP range was used between 0.05 and 1 mM and H_2O_2 was added during this work at concentrations between 1 and 10 mM.

2.4. Analyses of the irradiated solutions

The absorption of the solutions was followed in a Hewlett-Packard 38620 N-diode array spectrophotometer. The total organic carbon (TOC) was measured with a Shimadzu 5000 TOC analyzer. The disappearance of 4-CP was monitored with a high-pressure liquid chromatograph (HPLC) from Varian Corporation provided for with a 9065 diode. A Phenomenex C-18 inverse phase column was used in the HPLC and the eluent mobile phase consisted of water (30%) and acetonitrile (70%). The peroxide concentration in the aqueous solutions was measured using Merckoquant® paper from Merck AG, Switzerland. Reagents for the determination of Cl^--ions were obtained from Merck AG Cat KGaA (OC330408) containing Fe(III)-nitrate and $Hg(SCN)_2$ solutions. The absorbance of $Fe(SCN)^{2+}$ was measured at λ = 450 nm. At this wavelength, the Cl^--ion forms a complex by displacing the SCN^- from $Hg(SCN)_2$. The range of the Cl^--ion determination varied between 1 and 200 mg L^{-1}.

2.5. Infrared spectroscopy (FTIR)

Fourier transform infrared FTIR data were acquired on a spectrometer with a resolution of 4 cm^{-1}. Each FTIR spectrum consisted of 256 scans. The spectra were taken from the catalyst-loaded KBr tablets. The differential spectrum was obtained by the subtraction of FTIR spectrum of the glass from the spectrum found for the sample.

2.6. X-ray photoelectron spectroscopy (XPS)

The XPS was performed using Mg Kα radiation. The electron energy analyzer (Leybold EA200) was operated with band pass energy of 75 eV in the pre-selected transmission

mode. The binding energies of the surface elements of interest were referenced to the $Au4f_{7/2}$ signal of 84.0 eV according to the SCA A83 standard of the National Physics Laboratory [16]. The evaluation of the binding energies (BE) for the most important elements of the catalyst surface was carried out following standard procedures. A reproducibility of ±5% was attained in the XPS measurements. The ADS100 set was utilized to evaluate the XPS data by subtraction of X-ray satellites applying the background correction according to Shirley [17]. The effect of electrostatic charging effects was compensated by changing the electrostatic potential at the aperture site of the electron energy analyzer. The sputtering related to the depth profile may not exactly correspond to the true states in the glass/Ti, since the Ar-ion changes somewhat the nature of the membrane. This means that results of the erosion of the TiO_2 layers are valid while comparing one sample to the other under the same experimental conditions.

2.7. X-ray diffraction measurements (XRD)

The crystallographic phase of the TiO_2 on the glass rings was measured with a Siemens D500 diffractometer equipped with a copper anode and a graphite secondary monochromator.

2.8. High-resolution electron microscopy (HRTEM)

High-resolution transmission electron microscopy (HRTEM) was performed with a Philips XL 30 SFEG. For these observations, the TiO_2 Degussa P25 was removed from the glass using a razor blade to avoid excessive electric charge of the sample. The TiO_2 particles were deposited on a carbon-coated copper TEM grid. The high-resolution images were taken at 5 kV on the TiO_2 removed from the glass rings and deposited carbon film coating a TEM Cu-grid.

2.9. Atomic force microscopy of supported TiO_2 (AFM)

The AFM images were obtained using an atomic force microscope of AutoProbe M5 (ThermoMicroscopes Inc.). The intermittent contact mode and silicon cantilever with conical tip force constant was used having 13 N/m and a resonant frequency 280 KHz. All scans were performed with a set-point amplitude of 25 nm and at a scanning rate 0.5 Hz. This insured stable tip radius and no sample wear during the experiments. Images were flattened by a line-by-line (3rd order polynomial fit) using ThermoMicroscopes's image processing software and from these data the roughness was calculated.

3. Results and discussions

3.1. Infrared spectroscopy of the SiO_2-PO_4^{3-}-TiO_2 catalyst

Fig. 1 shows the differential spectra of the sample obtained by the subtraction of the FTIR spectrum of the glass from the FTIR spectrum of the SiO_2-PO_4^{3-}-TiO_2 catalyst. The insert of Fig. 1 shows FTIR spectrum of the catalyst. The differential spectrum shows a broad P–O stretching band between 1000 and 1200 cm^{-1}. This broad is assigned to the P–O stretching mode characteristic of the phosphonate group adsorbed on the RRs [18,19]. The weak P=O stretching band near 1200–1250 cm^{-1} suggests the coordination of the phosphoric oxygens to surface Lewis acid sites with electron delocalization [1]. The phosphonates have been shown to form complexes with cations and chelate metallic-ion [1–4]. But no analytical detailed information about the speciation of phosphonates for Ti is yet available [1,20].

3.2. Electron microscopy studies

Fig. 2 shows the particles of TiO_2 on the RR surface. The TiO_2 P25 Degussa particles were observed to have different

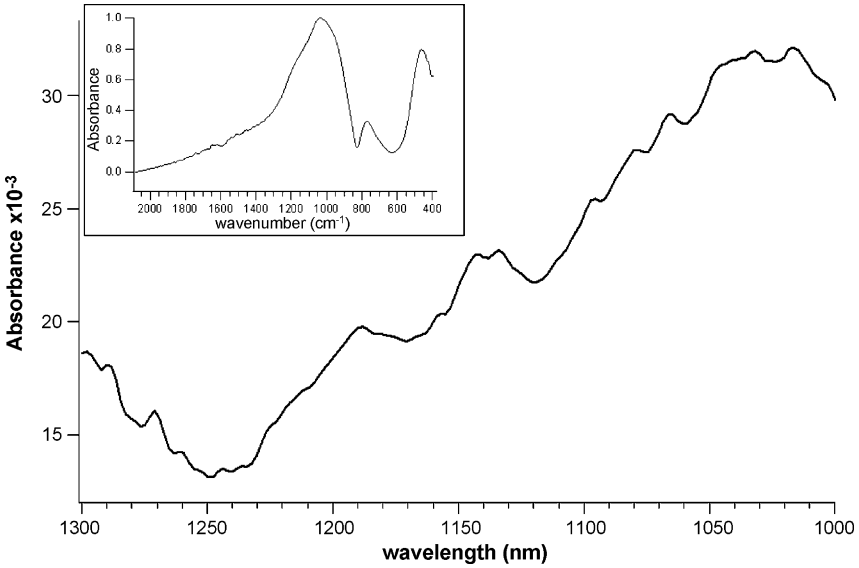

Fig. 1. Differential spectra of the surface layer obtained by the subtraction of the FTIR spectrum of the glass from the FTIR spectrum of the SiO_2-PO_4^{3-}-TiO_2 catalyst. The insert to figure shows the FTIR spectrum of the catalyst.

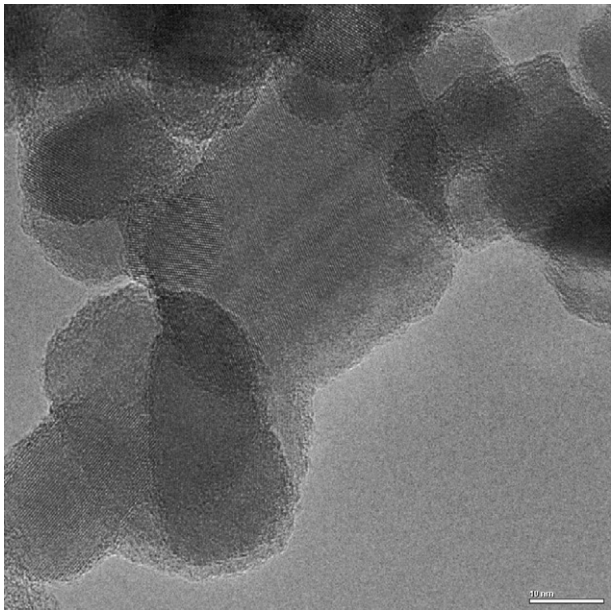

Fig. 2. High-resolution electron microscopy of the TiO_2 particles on the RRs.

shapes and sizes between 25 and 35 nm. Fig. 2 also shows the details of the inter-atomic planes of Ti in the TiO_2. The distance between these inter-atomic planes has been reported to be 0.55 nm [21].

3.3. X-ray diffraction studies

The diagram shown in Fig. 3 shows the most pronounced TiO_2 anatase peaks at 25.3° as referenced in the JCPDS file 84–1286 [22]. Fig. 3 also shows the minor rutile peaks for the TiO_2 Degussa P25. The intensity of these peaks follows the amount of the two crystallographic phases reported for TiO_2 Degussa P25. It is interesting to note that the last calcination step in the preparation of the SiO_2-PO_4^{3-}-TiO_2 composite

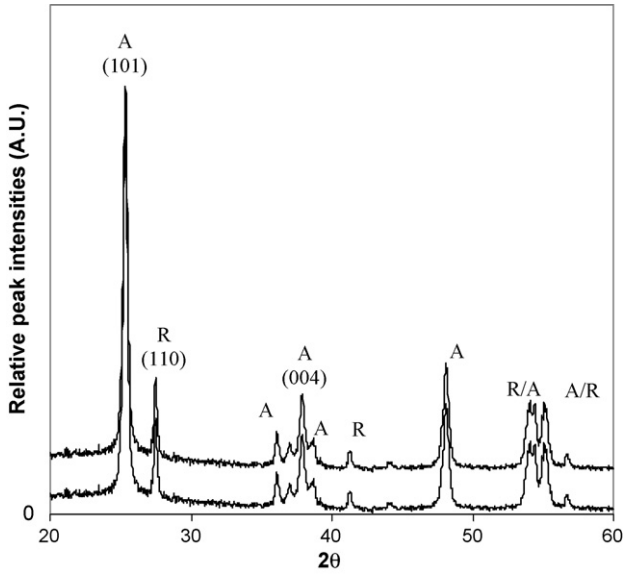

Fig. 3. X-ray diffraction diagram of the TiO_2 on the surface of the RRs.

catalyst when 500 °C is applied for 10 h does not convert the anatase of the TiO_2 Degussa P25 on the Raschig glass surface into rutile (see Section 2.2). In preparative TiO_2 powder technology heating for 10 h at 500 °C leads to the transformation of anatase to rutile. In the present study, as shown in Fig. 3, the anatase phase of the TiO_2 Degussa P25 is present. Therefore, the RRs have a structure forming function slowing down or precluding the transformation of anatase to rutile at the temperature used to prepare the catalyst (500 °C) within the heating time (10 h).

3.4. X-ray photoelectron microscopy studies (XPS)

Table 1 presents the surface percentage of the most important elements in the ten topmost layers (∼2 nm) of the composite SiO_2-PO_4^{3-}-TiO_2 catalyst. Table 1 shows that the amount of Si and Ti decreases only slightly within the 2 h needed for 4-CP photodegradation. The elements found other than Ti and O like C originate from atmospheric C and from impurities introduced during the catalyst preparation by 1-tertadecyl-phosphonic acid and other reagents.

The C on the surface was observed to increase only marginally due to some C-compound formation not rapidly removed from the catalyst surface. The catalyst is efficient during removal of 4-CP since it does not allow the accumulation of C on its surface. No surface accumulation of Cl was observed either after 2 h reaction since the level of Cl remained below the detectable limit of the XPS measurement. No P leached out of the photocatalyst during the 4-CP abatement as shown by the initial and final values for P in Table 1. Fig. 7 confirms the stability of the catalyst since repetitive 4-CP photodegradation was observed to proceed at the same pace in repetitive cycles. The O-content remains almost constant indicating that no oxygen containing species accumulate on the catalyst surface during the photocatalysis.

A small shift in the binding energy (BE) of Ti was observed after 2 h photocatalysis. The Ti 2p doublet shifted 0.3 eV. No asymmetric peaks were observed at the low edge of the doublet showing the formation of Ti^{3+} due to the $TiO_2e^-_{cb}$ generated under light irradiation. The observed shift in the Ti binding energies may involve changes in the relative amounts of TiOH and adsorbed water within the photocatalysis time [16,23].

Table 1
Initial and final surface percentage composition of the SiO_2-PO_4^{3-}-TiO_2 at time zero and after 2 h phtocatalysis of 4-chlorophenol

Elements	Initial (tetradecylphosphonic acid + Degussa P25)	Final (tetradecylphosphonic acid + Degussa P25)
Na 1s	1.55	0.29
F 1s	0.27	0.24
O 1s	64.3	65.6
Ti 2p	14.9	13.9
Si 2p	4.57	4.54
C 1s	6.98	7.68
P 2p	6.08	7.22
Cl 2p	<0.2	<0.2

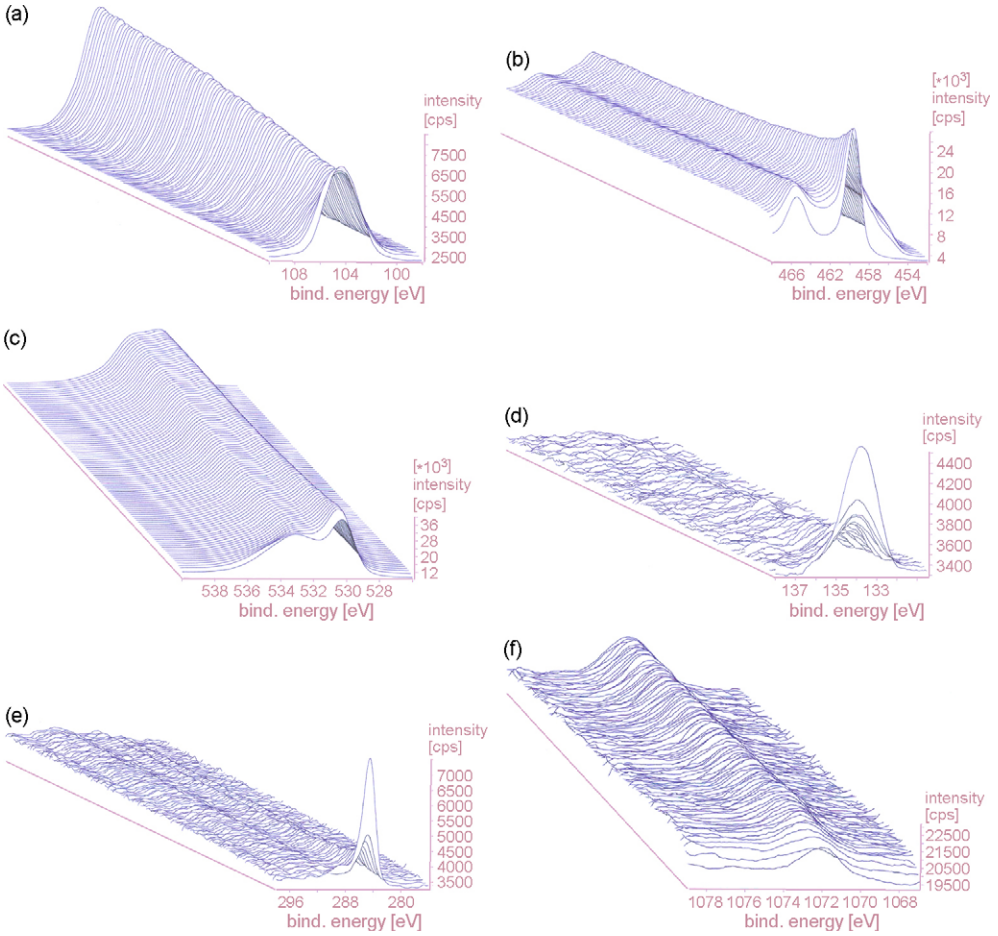

Fig. 4. (a) Depth profile of an Ar sputtered SiO_2-PO_4^{3-}-TiO_2 sample showing the Si layer distribution. (b) Depth profile of an Ar sputtered SiO_2-PO_4^{3-}-TiO_2 sample showing the Ti layer distribution. (c) Depth profile of an Ar sputtered SiO_2-PO_4^{3-}-TiO_2 sample showing the O layer distribution. (d) Depth profile of an Ar sputtered SiO_2-PO_4^{3-}-TiO_2 sample showing the P layer distribution. (e) Depth profile of an Ar sputtered SiO_2-PO_4^{3-}-TiO_2 sample showing the C layer distribution. (f) Depth profile of an Ar sputtered SiO_2-PO_4^{3-}-TiO_2 sample showing the Na layer distribution.

Fig. 4a shows the SiO_2-PO_4^{3-}-TiO_2 after the erosion of the 100 topmost layers due to 5 keV Ar^+-ions sputtering. Fig. 4a–f shows the XPS depth profile up to about 100 layers taking each layer with an average thickness of ~2 Å. The third axis in Fig. 4a–f shows the catalyst layers sputtered away due to the Ar-sputtering. Our computer graphic attached to the XPS recording system does not allow to insert the caption to this axis.

Taking into consideration the complexity of the surface in the composite SiO_2-PO_4^{3-}-TiO_2 catalyst, the value of 2 Å for the layer thickness is an approximate value since (a) preferential sputtering effects cannot be excluded [16,23] and (b) the layer thickness for each of the elements investigated depends on its particular sensitivity factor. Fig. 4a shows that the Si 2p peaks decrease slowly in the last 40–50 layers due to the grafting of TiO_2-PO_4^{3-} on the RRs. Fig. 4b shows the Ti 2p doublet for the 7–8 topmost layers with the Ti-content increasing towards the catalyst surface. The XPS signals of the O 1s doublet in Fig. 4c show components at 530.2 and 532.4 eV. Partial O-enrichment was observed after photocatalysis (see Table 1) due to the addition of H_2O_2 during 4-CP abatement. Fig. 4d shows the depth profile of P. The P 2p peak shoots up drastically within the last 5 layers due to the addition of 1-tetradecyl-phosphonic acid used during the preparation of SiO_2-PO_4^{3-}-TiO_2. Fig. 4e shows the second C1s peak at 284.6 eV corresponding to C from (a) the atmospheric CO_2 contaminating the catalyst surface and (b) the C-impurities present in the reagents used to prepare the catalyst (see Section 2.2). Fig. 4f shows that the Na-level in the catalyst seems to be evenly distributed within the sputtered top 100 catalyst layers. The Na-cation was observed to be a much more abundant cation relative to Ca and K.

3.5. Atomic force microscopy studies (AFM)

The AFM study of the SiO_2-PO_4^{3-}-TiO_2 supported catalyst allows to make some comments on the morphology of the catalyst surface at time zero and after 4-CP photodegradation. The cantilever in the AFM measurements applies a force of 0.1 Nw/m between the tip of the cantilever and the sample within a surface of 10–15 nm. The root mean square roughness (Rq) in Fig. 5 and the height difference between the highest and lowest surface points revealed little difference for the catalyst before and after use. This means that the porosity of the sample is conserved during the photodegradation of 4-CP The root mean square roughness (Rq) or rugosity was of 771.4 nm and

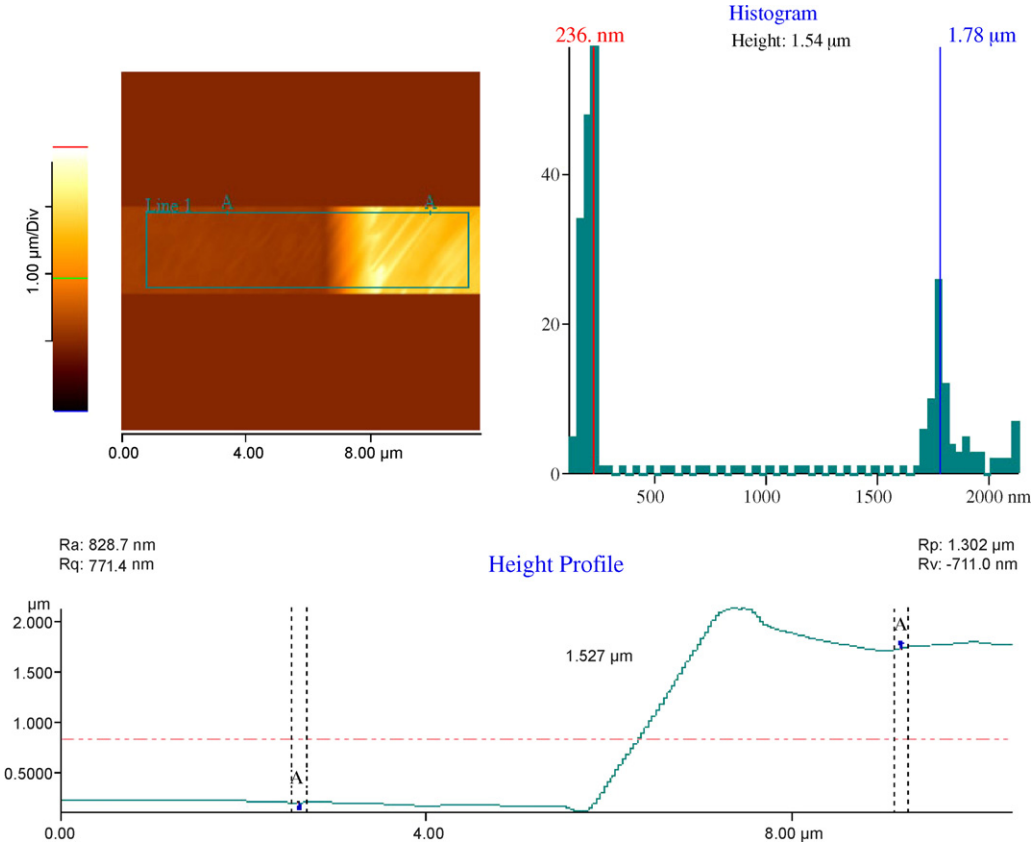

Fig. 5. Histogram of the layer showing the peaks of the coating in the projected area of 10 × 10 µm.

the average roughness (Ra) was determined to be 828.7 nm. The average roughness Ra value is seen to be different to Rq. Since Rq contains squared terms, large deviations from the average z height weigh more heavily than it is the case for the calculation of Ra. For the same reason, small deviations are given less weight in the calculation of Rq than Ra.

Fig. 5, upper left-hand side shows the AFM of a projected area of 10 µm × 10 µm. The clear rectangle in the middle section of the AFM image is taken to compute the height and the distribution of the peak heights from 0 to 2 µm. The results are shown in the histogram in the right-hand side in Fig. 5. The x axis of the histogram refers to the height distribution of the catalyst surface. The values noted at the left and right of the histogram of 236 nm and 1.78 µm represent the positions of the cursor and the height of 1.54 µm is the difference between the last two values.

The lower half of Fig. 5 shows the profile of the coating layer within a length of 10 µm. Between the broken double lines A and A, the maximum of the peak 2.013 µm was found by the addition of the peak height Rp 1.302 µm and Rv (low valley limiting value) of −711 nm or 0.711 µm. The broken line at 1.527 µm is the average height of the catalyst layer on the glass surface.

3.6. Photodegradation of the model compound 4-CP mediated by SiO_2-PO_4^{3-}-TiO_2.

Fig. 6a shows the disappearance of 4-CP in aqueous suspensions under medium pressure mercury lamp irradiation in the presence of H_2O_2 (10 mM) for different photocatalysts: (a) SiO_2-PO_4^{3-}-TiO_2 in the dark, (b) TiO_2 Degussa P25 in the dark, (c) solution of 4-CP in the dark as a control run, (d) solutions of 4-CP under light, (e) TiO_2 Degussa P25 under light, (f) SiO_2-PO_4^{3-}-TiO_2 under light and (g) Cl^--ions generation under light. It is readily seen that in the dark in the presence or absence of photocatalyst, no degradation of 4-CP was possible. Photolysis leads 4-CP disappearance; adding peroxide (trace d) accelerates the photocatalysis with TiO_2 Degussa P25 (trace e) and even more when using the innovative catalyst SiO_2-PO_4^{3-}-TiO_2. The catalyst mediates the 4-CP disappearance in ∼15 min and this time is shorter compared to suspensions of TiO_2 Degussa P25. The screening effect of the TiO_2 Degussa P25 suspension decreases significantly the light absorption compared to the SiO_2-PO_4^{3-}-TiO_2 rings. The TiO_2 Degussa P25 suspension (1 g L^{-1}) contained 50 mg of TiO_2 suspended in 50 mL, while the 30 g-coated RRs have been determined by elemental analysis (EA) to be coated with 75 mg TiO_2. Therefore, the amount of TiO_2 responsible for the photocatalytic effect is similar in both cases. But the surface dispersion of the TiO_2 on the rings and the higher light penetration makes for a more favorable catalytic performance in the case of SiO_2-PO_4^{3-}-TiO_2 rings. An added advantage is that the supported catalyst does not need to be separated from the solution after treatment. During the run shown in Fig. 6a, the pH value decreased from 8.0 to 4.6. The shift towards more acidic pH values is due to the HCl generated during the

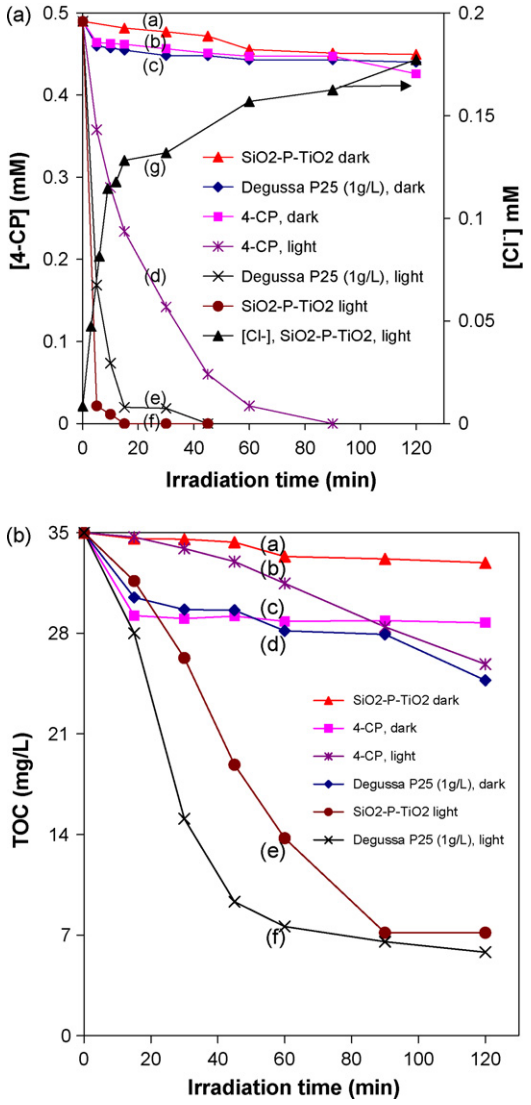

Fig. 6. (a) 4-CP disappearance under mercury light irradiation (400 W) as a function of time as determined by HPLC. Initial solution was pH 6.5. The Cl^--ion generation during the reaction is also indicated on the right-hand axis. (b) TOC decreases for solutions of 4-CP (0.49 mM) as a function of time under mercury light irradiation. For details see caption to the Figure.

4-CP degradation process

$$C_6H_5ClO + 13/2O_2 \rightarrow 6CO_2 + 2H_2O + HCl \quad (1)$$

The precursor of HCl in reaction (1) is the Cl^- anion generated in solution as shown in Fig. 6a, trace g, right-hand axis). The shape of the Cl^--ion generated in solution (trace g) suggests a complicated mechanism during 4-CP degradation [13].

$$C_6H_5ClO + e^-_{cb} \rightarrow C_6H_5O^\bullet + Cl,^- \quad E^o = 0.8-1.2 \quad (2)$$

The $C_6H_5O^\bullet$ radicals interact with the oxidative species formed on the surface of TiO_2 (IEP 7.0) that moves to more acidic pH values during the course of the reaction and becomes $TiOH_2^+$.

The abatement of 4-CP has been measured by HPLC and reported in Fig. 6a. The trend indicated increased abatement kinetics of 4-CP for the traces of (d) only light irradiation, (e) when Degussa P25 was used under light and (f) when SiO_2-PO_4^{3-}-TiO_2 was used under light. Fig. 6b shows that the traces (e and f) during the TOC reduction of 4-CP follow a reverse order as the one shown in Fig. 6a. Therefore, the abatement of 4-CP and the abatement of 4-CP and intermediates follow two distinctly different processes as it has been reported for many other organic compounds.

3.7. Long-term stability of the SiO_2-P-TiO_2 photocatalyst performance

Fig. 7 shows the true catalytic nature of the 4-CP abatement. The four first cycles are shown for the pollutant degradation. The catalyst was washed after each cycle and then the oxidant and 4-CP were added again in solution. Highly oxidative radicals are produced on the TiO_2 under light illumination. The surface of the TiO_2 is stepwise cleaned from impurities and more active sites become available to generate the radicals active in the abatement of 4-CP. This explains the acceleration during the abatement of 4-CP reported in Fig. 7. The catalyst was used over several months without variation in its kinetics or efficiency (amount of 4-CP degraded).

3.8. Light intensity dependence of 4-CP disappearance

Fig. 8 shows the disappearance of 4-CP as a function of light intensity. It is readily seen that the 4-CP disappearance in solution is more efficient as the intensity of the applied light is increased. The TOC reduction shown in the insert is favored by an increase of the applied light intensity. This implies that the saturation of TiO_2 acting as a photosensitizer on the SiO_2-PO_4^{3-}-TiO_2 rings has not been reached. The intensity of the mercury light used was decreased by using neutral gray grid filters to attenuate the incident light reaching the wall of the reactor.

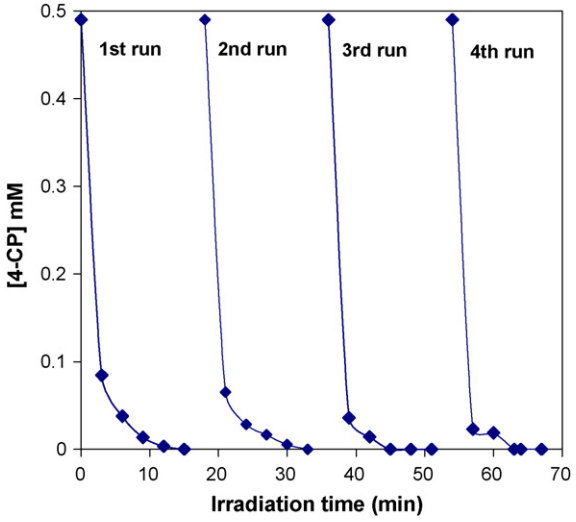

Fig. 7. Repetitive photocatalytic abatement of 4-CP under mercury light irradiation (400 W) photocatalyzed by SiO_2-PO_4^{3-}-TiO_2 in the presence of H_2O_2 (10 mM).

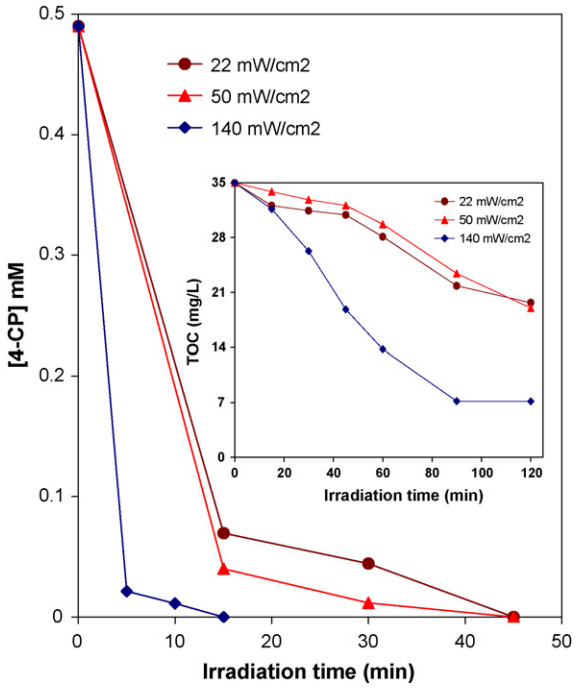

Fig. 8. Disappearance of 4-CP (0.49 mM) photocatalyzed by SiO_2-PO_4^{3-}-TiO_2 in the presence of H_2O_2 (10 mM) under mercury light irradiation as a function of the light intensity reaching the reactor wall. The insert shows the decrease of TOC for 4-CP.

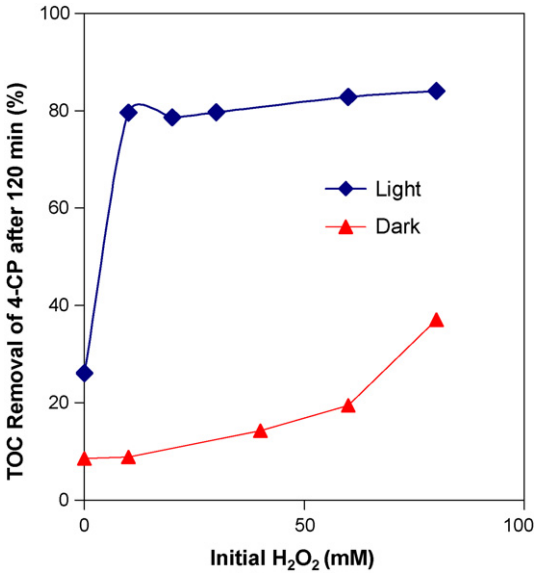

Fig. 9. TOC removal for a solution of 4-CP (0.49 mM) as a function of H_2O_2 concentration in the dark and under mercury light (400 W) in the presence of SiO_2-PO_4^{3-}-TiO_2 photocatalyst.

3.9. Effect of the H_2O_2 concentration on the TOC decrease of 4-CP solutions

It is readily seen in Fig. 9 that under mercury light irradiation about 27% of the initial 4-CP of the TOC was removed within 2 h when no H_2O_2 was added in solution (see Eq. (4) below). When the H_2O_2 is added up to 10 mM, the TOC removal was accelerated due to the additional radicals generated by the H_2O_2 decomposition in contact with TiO_2 (see Eq. (5) below) [24,25]. Above H_2O_2 (10 mM) further acceleration of the TOC removal was not observed since the scavenging of the OH-radical in solution reaction sets in

$$H_2O_2 + OH^o \rightarrow H_2O + HO_2{}^o \quad (3)$$

Fig. 9 shows the TOC conversion of the 4-CP aromatic ring by oxidative radicals (Eq. (4)) and due to the radicals formed upon addition of H_2O_2 (10 mM)). The reactions leading to $HO_2{}^o$ and OH^o under light irradiation in aqueous solutions have been extensively reported [9,10]

$$e\text{-}_{cb} + O_2 \rightarrow O_2{}^- + H^+ \rightarrow HO_2{}^o \quad (4)$$

$$e\text{-}_{cb}\text{-} + H_2O_2 \rightarrow OH^- + OH^o \quad (5)$$

3.10. Effect of the 4-CP concentration on the photodegradation kinetics

Fig. 10 shows the 4-CP disappearance is a function of its initial concentration added in solution. As expected, a lower 4-CP concentration is abated in shorter times. The steeper decline observed at a higher 4-CP concentration was due to the more favorable mass transfer taking place between the 4-CP and the TiO_2-coated rings. The mass transfer between the solution and the photocatalyst is driven by the difference in the 4-CP concentration existing between the bulk of the solution and the catalyst at the RR interface. The diffusion length (x) for the oxidative radicals away from the catalyst surface can be estimated from the simplified Smoluchowski diffusion relation

$$x^2 \sim D \times \tau. \quad (6)$$

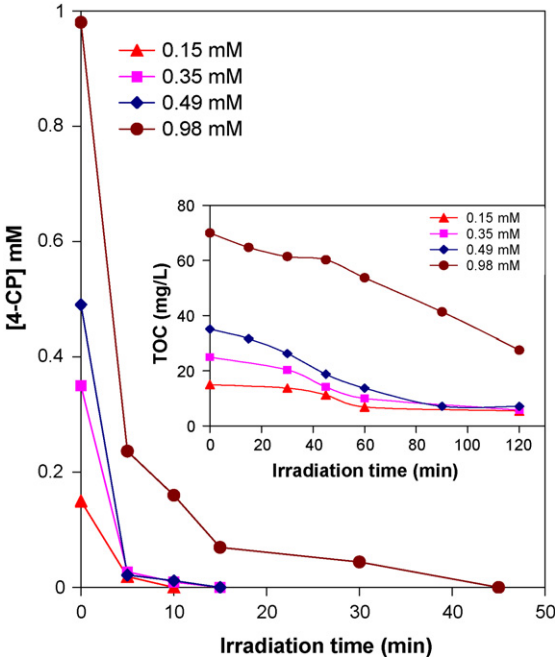

Fig. 10. Disappearance of 4-CP in solution under mercury light (400 W) in the presence of H_2O_2 (10 mM) and of the SiO_2-PO_4^{3-}-TiO_2 catalyst as a function of the of the concentration of 4-CP in solution. The insert shows the TOC decrease.

The reaction rate between the OH^o radical and 4-CP has been reported to be close to $10^9\ M^{-1}\ s^{-1}$ [14]. At a concentration of 4-CP (0.20 mM), the lifetime of the encounter pair τ is $\sim 10^{-6}$ s. For a concentration of 4-CP of 0.20 mM, the inverse lifetime of the encounter-pair can be estimated: $1/t = 0.20\ 10^{-3}\ M \times 10^9\ M^{-1}\ s^{-1} \approx 10^6$ s and the lifetime of the 4CP-$OH_{radical}$ encounter pair is found to be $\sim 10^{-6}$ s. With D $\sim 5\ 10^{-6}\ cm^2\ s^{-1}$, a value for the diffusion length (x) of $\sim$50 nm by Eq. (6) is found for the OH^o radical away of the catalyst surface. For the $HO_2{}^o$ radical, the reaction rate of $HO_2{}^o$ with 4-CP has been determined to be in the range of $\sim 10^6\ M^{-1}\ s^{-1}$ [13]. From this a value of $\sim$310 nm can be estimated for the diffusion length $HO_2{}^o$ radical away from the catalyst interface.

4. Conclusions

This study shows that the photocatalytic destruction of 4-CP on SiO_2-$PO_4{}^{3-}$-TiO_2 RRs is possible and presents the following features: (1) the catalyst is capable to induce the full degradation of 4-CP within the minute range. The catalyst is non-toxic and relatively lower in cost, (2) the catalyst presents acceptable kinetics for 4-CP degradation under low intensity mercury arc light (22 mW cm^{-2}) using a mild oxidant H_2O_2, (3) the treated solutions do not need an end-of-pipe separation and finally (4) no remobilization of Ti was observed in solution showing that the catalyst is resistant to the highly oxidative radicals produced in solution.

Acknowledgments

We gratefully acknowledge the financial support of CTI TOP-NANO 21 under Grant No. 5960.1(Bern, Switzerland) and COST Action 540 PHONASUM ‘‘Photocatalytic technologies and novel nano-surface materials, critical issues’’ for the financial support of this study.

References

[1] G. Guerrero, H. Mutin, A. Vioux, Chem. Mater. 13 (2001) 4367.
[2] C. Maillet, P. Janvier, M. Pipelier, T. Praveen, Y. Andres, B. Bujoli, Chem. Mater. 13 (2001) 2879.
[3] D. Protet, B. Denisot, E. Rump, J. Leujene, P. Jallet, J. Coll. Inter. Sci. 238 (2001) 37.
[4] R. Michel, W. Lussi, G. Csucs, I. Reviakine, G. Danuser, B. Keterer, A. Hubbell, M. Textor, D. Spencer, Langmuir 18 (2002) 3281.
[5] Th. Oppenlaender, Photochemical Purification of Water and Air, Wiley V-Ch, Weinheim, Germany, 2003.
[6] G. Winkler, Titanium Dioxide, Vincent Verlag, Hannover, Germany, 2003 .
[7] M. Dhananjeyan, J. Kiwi, R. Thampi, Chem. Commun. (2000) 1443.
[8] A. Bozzi, I. Guasaquillo, J. Kiwi, Appl. Catal. B. 51 (2004) 201.
[9] A. Fujishima, T. Rao, D. Tryk, J. Photochem. Photobiol. C, Rev. 1 (2000) 1.
[10] A. Mills, J. Photochem. Photobiol. A 152 (2002) 233.
[11] M. Kaneko, I. Okura (Eds.), Photocatalysis: Science and Technology, Kodansha-Springer Verlag, Tokyo, 2002.
[12] U.G. Ahlborg, T.M. Thandberg, CRC Crit. Rev. Toxic. 53 (1999) 131.
[13] M. Pera-Titius, V. Garcia-Molina, M. Banos, J. Gimenez, S. Esplugas, Appl. Catal. B. 47 (2004) 219 (and references therein).
[14] J. Bandara, J. Mielczarski, A. Lopez, J. Kiwi, Appl. Catal. B. 34 (2001) 321.
[15] M.-P. Ormad, J.L. Ovelleiro, J. Kiwi, Appl. Catal. B. 32 (2001) 157.
[16] D. Briggs, M. Shea, second ed., Practical Surface Analysis, vol. 1, John Wiley, Chichester. UK, 1990.
[17] A. Shirley, Phys. Rev. B. 5 (1979) 4709.
[18] W. Gao, C. Dickinson, C. Grozinger, G. Morin, L. Reven, Langmuir 12 (1996) 6429.
[19] Sh. Pawsey, K. Yach, L. Reven, Langmuir 18 (2002) 5205.
[20] B. Nowack, Water Res. 37 (2003) 2533.
[21] R.D. Shanon, Acta Cryst. A32 (1976) 751.
[22] JCPDS Powder Diffraction Files, International Center for Diffraction Data, Swathmore, PA, USA, 1969.
[23] D. Wagner, Handbook of X-ray Photoelectron Spectroscopy, Perkin-Elmer Corp., 6509 Flying Cloud Drive, Eden-Prairie, Min. 55534, USA, 1989.
[24] R. Bacsa, J. Kiwi, Appl. Cat. B. 16 (1998) 19.
[25] L. Minsker, C. Pulgarin, P. Peringer, J. Kiwi, N. J. Chem. 18 (1994) 897.